DEVELOPMENTAL DYNAMICS 235:68–81, 2006

RESEARCH ARTICLE

Epithelial Transformations in the Establishment of the Blood–Gas Barrier in the Developing Chick Embryo Lung

A.N. Makanya,[1,2] R. Hlushchuk,[2] H.-R. Duncker,[3] A. Draeger,[2] and V. Djonov[2]*

The tall epithelium of the developing chick embryo lung is converted to a squamous one, which participates in formation of the thin blood–gas barrier. We show that this conversion occurred through processes resembling exocrine secretion. Initially, cells formed intraluminal protrusions (aposomes), and then transcellular double membranes were established. Gaps between the membranes opened, thus, severing the aposome from the cell. Alternatively, aposomes were squeezed out by adjacent cells or were spontaneously constricted and extruded. As a third mechanism, formation and fusion of severed vesicles or vacuoles below the aposome and their fusion with the apicolateral plasma membrane resulted in severing of the aposome. The atria started to form by progressive epithelial attenuation and subsequent invasion of the surrounding mesenchyme at regions delineated by subepithelial α-smooth muscle actin–positive cells. Further epithelial attenuation was achieved by vacuolation; rupture of such vacuoles with resultant numerous microfolds and microvilli, which were abscised to accomplish a smooth squamous epithelium just before hatching. ***Developmental Dynamics 235:68–81, 2006.*** **© 2005 Wiley-Liss, Inc.**

Key words: avian lung development; blood-gas barrier formation; secarecytosis; permerecytosis; epithelial attenuation

Accepted 16 September 2005

INTRODUCTION

In contrast to mammals, the mechanisms underlying development of the chick embryo lung have received little attention, probably due to the complex morphology of the avian lung. From a simple lung bud at embryonic day 4 (E4), a complex gas-exchanging lung is accomplished by day 20–21 of incubation, when the chick emerges from the shell. This is a complex process, by which the epithelium of the avian lung in the sprouting parabronchi is converted from a tall columnar to a squamous one with an estimated harmonic mean thickness of the blood–gas barrier of 0.318 μm (Duncker and Guentert, 1985; Maina et al., 1989). This is just approximately half of that reported for the adult rat lung by Kalenga et al. (1995). Among the extant vertebrate taxa, the avian lung is reputed to be the most complex and efficient gas exchanger (Duncker, 1971; King and McLelland, 1989). The establishment of a thin blood–gas barrier by the time of hatching remains enigmatic, despite several studies on the developing avian lung (Gallagher, 1986a,b; Maina, 2003a,b, 2004). Earlier studies have established that the avian lung arises from the primitive pharynx at approximately 3–4 days after incubation (Duncker, 1978; Bellairs and Osmond, 1998). The pharyngeal endoderm gives rise to the bronchial system, the mesenchyme forms the muscles, connective tissue, and the lymphatics that accompany the bronchi (Bellairs and Osmond, 1998). The chick lung by E12 comprises blind ending outgrowths of the parabronchi surrounded by mesenchyme. The growing tips of the tertiary parabronchi bifurcate so that parabronchial cir-

[1]Department of Veterinary Anatomy, University of Nairobi, Nairobi, Kenya
[2]Institute of Anatomy, University of Berne, Berne, Switzerland
[3]Institute of Anatomy and Cell Biology, Justus-Liebig-University, Giessen, Germany
Grant sponsor: Bernese Cancer League; Grant sponsor: Swiss National Science Foundation; Grant number: 3100A0-104000/1.
***Correspondence to: Valentin Djonov, M.D., Institute of Anatomy, University of Bern, Balzerstrasse 2, 3000 Bern, Switzerland. E-mail: valentin.djonov@ana.unibe.ch**

DOI 10.1002/dvdy.20627
Published online 28 October 2005 in Wiley InterScience (www.interscience.wiley.com).

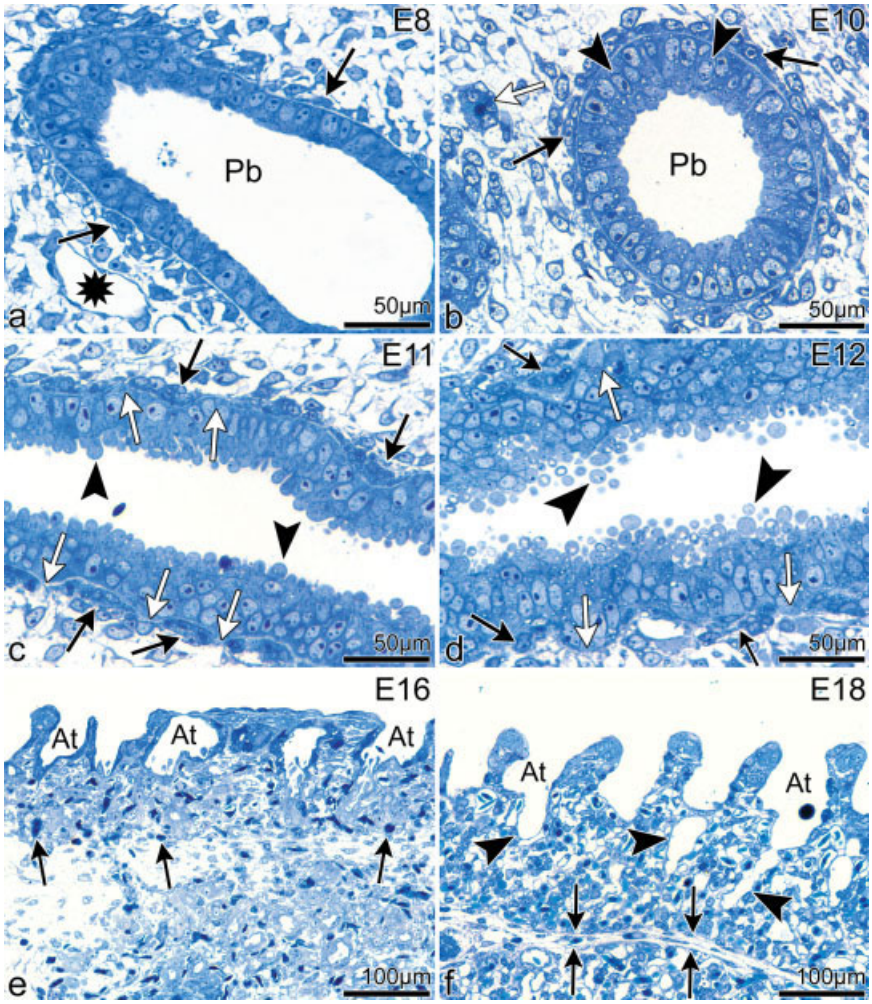

Fig. 1. Micrographs of semithin sections showing the structural changes in the parabronchial epithelium of the developing chick embryo lung between embryonic day 8 (E8) and E18. **a,b:** At E8, the parabronchi (Pb) were lined with a cuboidal epithelium, which became tapered by E10, and transformed to a high columnar one. The first signs of pseudostratification were depicted by apical relocation of some nuclei (black arrowheads in b). The surrounding mesenchyme contained occasional developing feeding and draining vessels (asterisk in a) and few blood capillaries (white arrowhead in b). Subepithelial cells became aligned along the basement membrane (black arrows in a and b). **c,d:** By E11 (c), the parabronchial epithelium was pseudostratified and the apical parts of the cells appeared club-like (arrowheads in c). By E12, these apical parts were severed such that they appeared to fall off into the parabronchial lumen (arrowheads in d). Notably, the arrangement of the subepithelial cells associated with the parabronchial basement membrane (BM) changed their continuous appearance (dark arrows), so that, from E11, regions of the BM devoid of such cells were detectable (white arrows). **e,f:** The atria (At) had already formed by E16, the epithelium had thinned out, and the number of vascular profiles (arrows in e) increased in the mesenchyme. At early E18, the infundibula (arrowheads in f) started to invade the mesenchyme. The interparabronchial septum was well formed (arrows in f).

cuits are formed by anastomoses of adjacent branches (Jones and Radnor, 1972; Duncker, 1971, 2000). The parabronchi by E13 are hollow tubes lined by columnar cells and surrounded by mesenchymal tissue. Reportedly, the smooth cross-sectional outline of the tertiary parabronchi starts to disappear by E14 as outpouchings start to develop from the epithelium. These are made of epithelial strands, which become canalized, so that several diverticula arise from the central lumen.

During the late growth phase the parabronchi increase in girth, the atrial outpouchings form and give rise to a network of air capillaries. There is reduction of the epithelial cells of the air capillaries to squamous type, while in the atrial region the cells are converted to granular pneumocytes or avian inclusion body cells (Jones and Radnor, 1972). Lung development has been revisited recently by Maina (2003a) with the observations that parabronchi sprout from secondary bronchi from E8, become encircled by mesenchymal cells and by E13, the basement membrane becomes conspicuous. At around this time, parabronchial epithelial cells tend to project into the lumen; posses microvilli, club-like and arm-like process in addition to having abundant intercellular spaces (Maina, 2003a). The latter author recently has shown that the thin barrier is formed by extensive attenuation of the epithelial cells as the air capillaries invade the mesenchymal tissue matrix (Maina, 2004). The latter event coupled with mesenchymal tissue degradation brings the air capillaries and the blood capillaries in close proximity (Maina, 2004). Scheuermann et al. (1998) indicated that superfluous cells of the developing parabronchial epithelium are discharged into the lumen and undergo vacuolar degeneration. However, the precise sequence of events and the driving forces leading to the morphophenotypes described above, as well as the mechanisms by which the tall columnar cells are converted into a rather thin and broad squamous epithelium of the blood–gas barrier are unknown. In the current study, we have investigated the processes characterizing the avian lung epithelial attenuation, from the time the parabronchi sprout to the time a thin blood–gas barrier is established. Unlike what has been reported before (Gallagher, 1986b), the chick lung uses strategies in its morphogenesis that are dissimilar to those that have been elucidated previously in developing mammalian organs. We report here that processes resembling exocrine secretion, albeit phenotypically distinct are adopted to attenuate the lung epithelium during embryological development.

RESULTS

During the early developmental stages the chicken lung was characterized by loose mesenchyme containing occasional isolated blood vessels and numerous developing parabronchi. The parabronchi underwent dra-

matic changes affecting both their three-dimensional structure as well as their epithelial morphology. An overview of the changing epithelial morphology in the developing lung is presented in Figure 1. At embryonic day 8 (E8), the epithelium of the parabronchial tubes was cuboidal to low columnar (Fig. 1a), becoming high columnar by E10, and at the same time, cells acquired pointed apices (Fig. 1b). From E11, cells with tapering luminal apices and debris of rounded cell blebs were encountered (Fig. 1c). Furthermore, the epithelium was transformed into a pseudostratified one, apparently due to multiplication and enlargement of epithelial cells such that some cells were squeezed out of phase. By E12, the nipping process continued so that these apical parts of the cells were severed and extruded into the parabronchial lumen (Fig. 1d). Some of the subepithelial cells changed their orientation and came to lie parallel to the basement membrane, forming a continuous layer at early stages, which later became interrupted by narrow gaps through which migrating epithelial cells of the incipient atria emerged (Fig. 1a–d). The parabronchi by E16 were no longer simple-surfaced cylinders, because the internal aspects were now interrupted by the formative atria (Fig. 1e). The atria arose probably by mesenchyme invasion and attenuation of the epithelium without additional proliferation. After the formation of the atria, at E18 (Fig. 1f) the mesenchymal invasion progressed by formation of multiple infundibula covered by very thin epithelium. At the same time point, the mesenchyme was massively reduced so that thin interparabronchial septa containing the major supplying and draining parabronchial vessels were formed.

An overview of the parabronchial mucosal surface with the scanning microscope between E10 and E19 revealed the progressive events of epithelial transformations and the development of the atria. At E10, the lumen was lined with tall apically tapering cells many of which bore club-like luminal protrusions (Fig. 2a). The tapering apices were progressively nipped, and by E12, they began to be liberated into the lumen (Fig. 2b). The first signs of atria formation were ev-

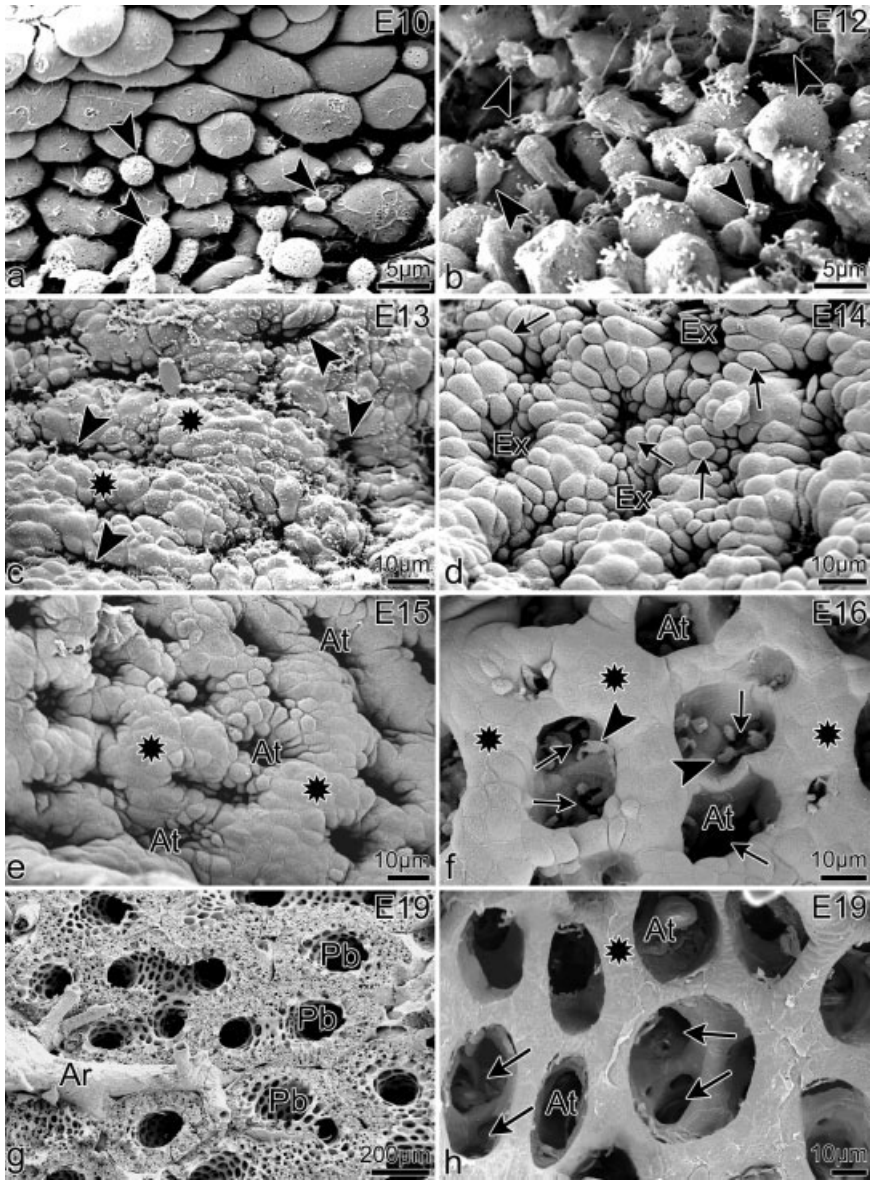

Fig. 2. Scanning electron photomicrographs of the embryonic pulmonary tissue illustrating the various changes characterizing the developing parabronchi between embryonic day 10 (E10) and E19. **a,b:** At E10, the parabronchial epithelium consisted of tall columnar cells with smooth rounded luminal apices. Occasional club-like protrusions of variable sizes were apparent (arrowheads in a). By E12, the epithelium was rather rugged and club-like apical protrusions at different stages of development were abundant (arrowheads in b). See also Figures 1 and 5 and 10 for comparison. **c,d:** An overview of the parabronchial mucosa at E13 and E14 revealed the progressive development of the atria. These inaugurated as shallow depressions on the mucosal surface (arrowheads in c) separated by ridges of the mucosa (asterisks in c) and gave the mucosa a folded appearance. By E14 (d), the depressions were converted to circular excavations (Ex) surrounded by irregularly shaped cells (arrows), which gave the surface of the intervening mucosa a rugged appearance. **e,f:** The atrial excavations (At) at E15 were much deeper, the surrounding cells became more regular in height and broadened, presenting a general flat surface (asterisks in e). By E16 (f), the atria had broadened tremendously and showed secondary depressions, which were the incipient infundibula (arrows in f). The floor of the nascent infundibula was characterized by sparse tall cells or portions thereof, projecting conspicuously above the general surface of the atrial floor (arrowheads in f). The mucosa between the atria was now remarkably smooth (asterisks). **g,h:** The pulmonary tissue at E19 generally resembled the structure of adult birds with almost evenly spaced parabronchi (Pb) lined by numerous openings to the atria (At). The interatrial septa (asterisk in h) had largely thinned out and separated the entrances to the contiguous atria (arrows in h). Notice also an artery (Ar in g), giving rise to interparabronchial vessels.

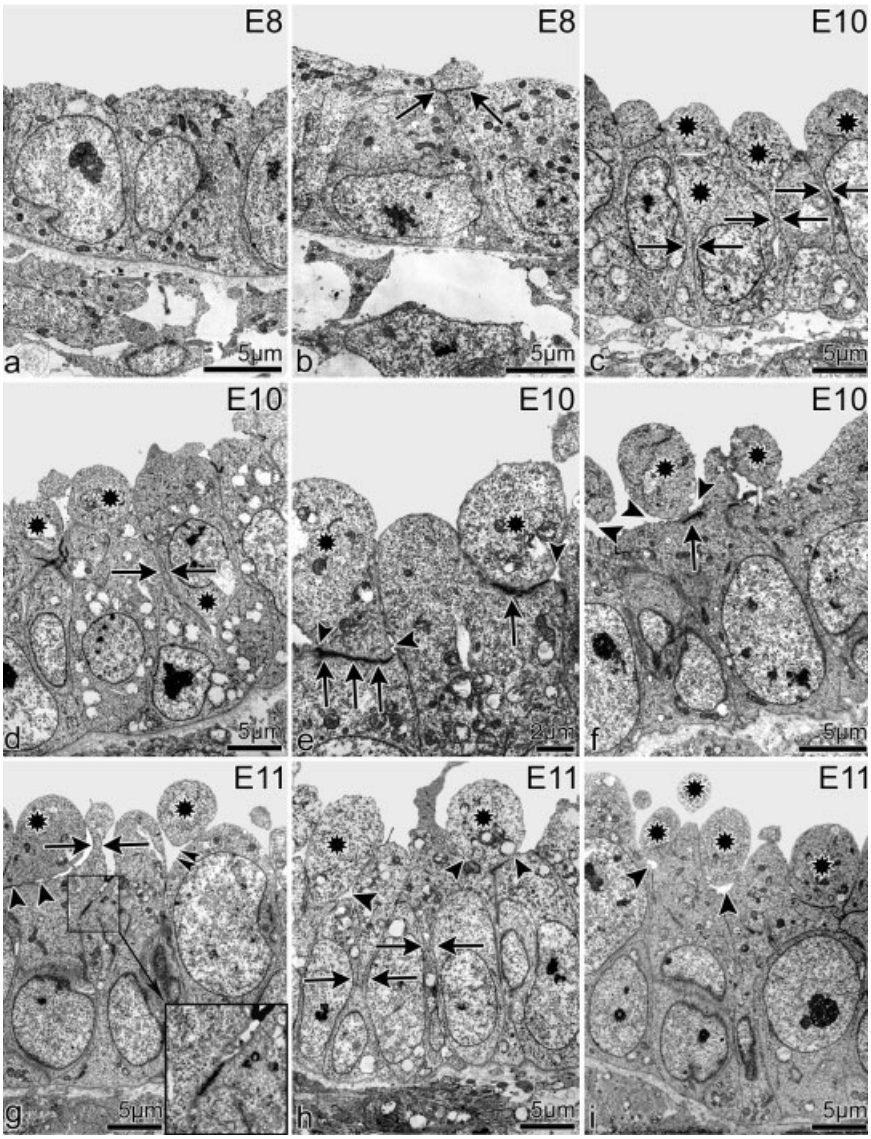

Fig. 3. Transmission electron microscopy (TEM) images illustrating the mechanisms involved in cell attenuation during parabronchial development between embryonic day 8 (E8) and E11. **a,b:** At E8, the epithelium was cuboidal to low columnar and the nuclei were mainly basal. Small dome-shaped cell projections, which were separated from the main cells by electron-dense bands (arrows in b), were occasionally encountered. The basement membrane was amorphous. **c–f:** By E10, some regions of the epithelium appeared pseudostratified and the apical parts of the cells demonstrated club-like formations (asterisks in c). Some cells appeared to squeeze out the apical portions of their neighbors (arrows in c, d). The development of transcellular electron-dense bands (arrows in e, f) was followed by separation of the double membranes (arrowheads in e, f), which extended the intercellular spaces, severing the apical parts of the cells from the basal ones to form attenuation bodies (cell blebs). **g–i:** The process of cell nipping (arrowheads) and squeezing by neighboring cells (arrows in h) was evident by E11 and contributed to the number of extruded attenuation bodies (asterisks). Opening of the intercellular spaces (double arrowheads in g and inset) shifted the intercellular junctions basally. Spontaneous constriction of the apical part of the cell (arrows in g) resulted in formation of club-like processes.

ident at E13. These began as shallow depressions on the mucosal surface lined by epithelial cells and separated by broad mounds of rugged mucosa, which gave the mucosal surface an undulating appearance (Fig. 2c). The epithelial invaginations deepened, so that by E14 they converted to circular excavations surrounded by irregularly shaped cells (Fig. 2d). The surface of the mucosa by E15 remained rugged but had less cellular debris and club-like cellular projections were restricted to the atrial depressions. The mucosa separating the various incipient atria at E15 started to become thinner and smooth, the foldings were lost, and only a few cells around the atrial openings showed irregular heights (Fig. 2e), and by E16, atria were well formed, the interatrial mucosa was smooth, and the infundibula started to form as depressions at the floor of the atria (Fig. 2f). The interatrial septa were uniformly smooth apart from the atrial floor where some cell processes jutted out prominently into the atrial lumen (Fig. 2f). The appearance of the lung at E19 resembled that described for the adult bird with regularly arranged parabronchi and intervening blood vessels (Fig. 2g). The internal surface of the parabronchi was characterized by evenly spaced atria, which further opened into the infundibula, and the mucosae were remarkably smooth (Fig. 2h).

The events, processes, and mechanisms that transformed the developing lung epithelium were captured in details at the transmission electron microscopy level. The progressive and successive epithelial alterations were monitored between E8 and E21 (Figs. 3, 5–8). The first signs were apparent at late E8 with the cells becoming morphologically polarized, i.e., they tapered toward the lumen and electron-dense bands appeared to separate the tapered apical part from the rest of the cell (Fig. 3a,b). By E10, the epithelium became tall columnar, tapering was accelerated, and the cells enlarged and appeared to squeeze their immediate neighbors (Fig. 3c,d). The electron-dense bands were seen to constitute a double membrane and, at such double membranes, the apical portion of the cell was separated from the basal part (Fig. 3e,f). Apical intercellular junctions opened up so that the apical portions (aposomes) of adjacent cells were clearly delineated (Fig. 3f). The cell separation became more prominent at E11 (Fig. 3g–i). Additionally, tapering apical parts of some cells were squeezed out by the better-endowed neighboring cells (Fig. 3h). Concomitant with these processes, apical intercellular spaces became broadened, separating the apical processes and in so doing pushed the apical cell junctions basally (Fig. 3g–i). The processes attendant to cell attenuation in the avian lung involved

cell cutting (secarecytosis) and cell pinching (peremerecytosis) as described below. During these two processes, apical tapering of cells and basal relocation of lateral cell junctions occur as demonstrated in Figure 3 by transmission electron microscopy and by Alexa–phalloidin staining for filamentous actin (f-actin) in Figure 4.

The first signs of atria formation were evident at E13 when the now stratified epithelium showed designated areas with accelerated cell nipping (Fig. 5a,b), mainly by the processes described above. Consequently, numerous rounded aposomal bodies were released into the parabronchial lumina (Fig. 5a,b). By E14, the epithelia had thinned out to irregular cuboidal in the formative atria, which were now invading the surrounding mesenchyme (Fig. 5c,d) and the epithelium was further reduced in size by cell nipping or loss of entire cells by squeezing. The epithelium by E15 had largely thinned out to low cuboidal with short microvilli (Fig. 5e). At the same time, the first infundibula started to form by excavation of the cuboidal epithelium (Fig. 5e,f).

As soon as the infundibula had been formed, they gave rise to the air capillaries by formation and subsequent fusion of intraepithelial vesicles, as may be inferred from the presence of many short microvilli (Fig. 5g). Often, cells located at the infundibular entrance at the bottom of the atria showed intraluminal projections of different sizes (Fig. 5h). The atrial epithelium at E16 had changed from cuboidal to low cuboidal. Some of the cells bore irregularly shaped apical processes jutting out into the lumen (Fig. 6). Subsequently, electron-dense bands developed at the bases of the projections, followed by spaces with the ultimate separation of the projection and formation of cell attenuation bodies (blebs; Fig. 6a–d). The projections appeared as club-like processes (Fig. 6d–h) projecting into the atrial space. Many such projections were severed by spontaneous strangulation, which involved progressive constriction of the basal part of such a portion of a cell (Fig. 6a–h). Some of the projections were severed by vesiculation and subsequent fusion as can be deduced from the many short microvilli on the remaining epithelium and on the discharged aposomes (Fig. 6a–d).

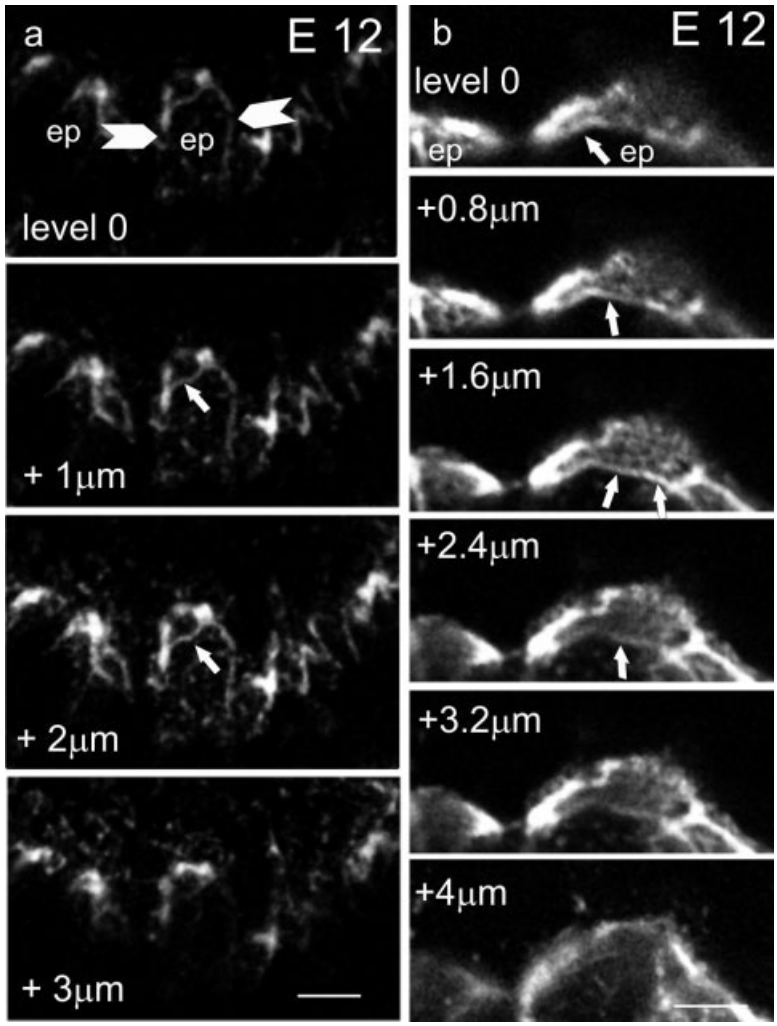

Fig. 4. Photomicrographs of serial sections of two parabronchi from embryonic day 12 (E12) chick embryos labeled with Alexa–phalloidin outlining actin filaments (a and b). The two series show tapered epithelial cells. Actin filaments delineate the apical and basolateral borders (arrowheads in a) of individual epithelial cells (ep) and mark the aposomal protrusion (arrows). At higher magnification (b), the aposomal body and the incomplete separation from its epithelial cell by a narrow actin demarcation line is visible (arrows in b). Scale bars = 5 μm m in a; 1.5 μm in b.

From E15, a new mechanism augmented the process of cell attenuation and this entailed formation of many small vacuoles in the epithelium (Fig. 7a–d), and in subsequent steps, the vacuoles enlarged and their membranes fused with the apical plasma membrane so that the vacuoles ruptured releasing their contents into the lumen. Rupturing of the vacuoles left many microfolds and microvilli of varying shapes and sizes on the apical plasma membrane. In an alternative step, contiguous vacuoles coalesced and fused with each other and with the lateral plasma membranes and in so doing cut off large parts of the apical portions of the cells with the result that more aposomal bodies were released into the lumen (Fig. 7e,f). The epithelia of air capillaries at E18 still contained many lamellar bodies (Fig. 8). Such lamellar bodies were extruded by bulging onto the apical plasma membrane with subsequent rupture of the membrane (Fig. 8b,c). Alternative methods of eliminating lamellar bodies entailed formation of vacuoles underneath the lamellar bodies with subsequent rupture of the vacuoles so that the lamellar bodies were discharged together with part of the cytoplasm (Fig. 8d). The by-products of epithelial attenuation, which

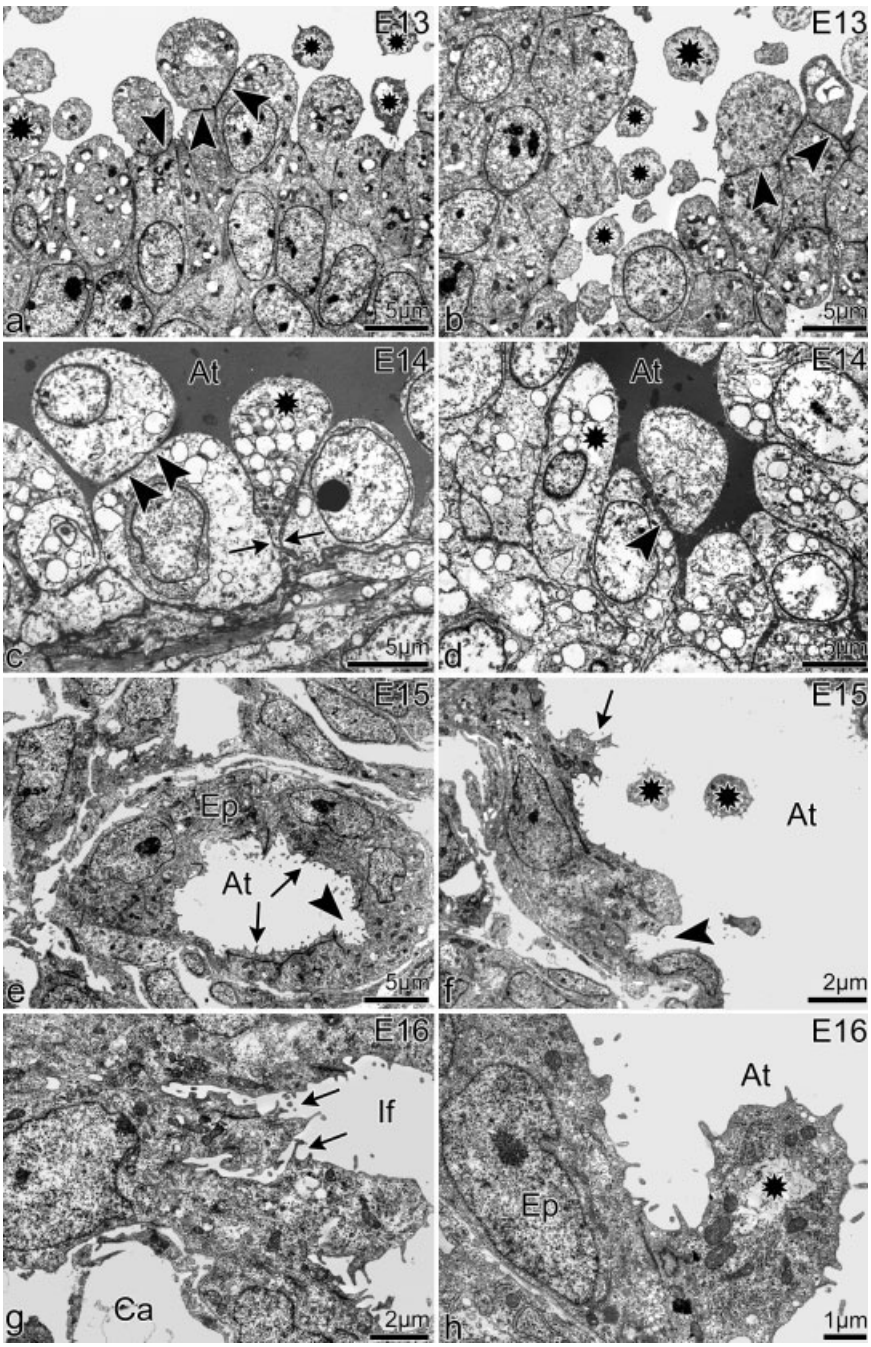

Fig. 5. Transmission electron photomicrographs illustrating the various mechanisms involved in initiation of atrial formation and further epithelial attenuation during parabronchial development. **a,b:** By embryonic day 13 (E13), the process of cell nipping (arrowheads) became accelerated so that the cell blebs in the lumen became numerous (asterisks). The epithelial excavation by the nipping process became exaggerated in the regions of the future atria so that shallow depressions with rounded cell blebs became apparent (see asterisks in b). See also Figures 1 and 2 for comparison. **c,d:** The atrial depressions became deeper by day 14, and the epithelium thinned out to irregular cuboidal as a result of progressive nipping (arrowheads) and squeezing (double arrows in c). Few cells still remained tall (asterisks) and jutted out into the atrial lumen. Notice that the lumen of the formative atria (At) as well as parabronchial lumen are filled with a dark staining fluid. **e,f:** The atrial epithelium had transformed to low cuboidal by E15 with an irregular luminal surface studded with short irregular microvilli (arrows) and showed the first signs of infundibula formation (arrowheads). The number of attenuation bodies (asterisks) in the parabronchial lumen was reduced. **g,h:** The first infundibula (If) and air capillaries (arrows) became evident at E15. The air capillaries started to invade into the epithelium (arrows) and tended to approach the blood capillaries (Ca). At this time point, sparse cell projections (asterisk in h) protruded into the atrial lumen and above the attenuating epithelium (EP). See also Figures 1 and 2 for comparison.

included lamellar bodies and cellular debris, were cleared by pulmonary macrophages (Fig. 8e). Notably at the time of hatching (E21), type II pneumocytes were restricted to the region of atrial openings (Fig. 7f). Further attenuation of the now low cuboidal epithelium proceeded through vesiculation as described above, an event that resulted in many microvilli and microfolds (Fig. 8a–d). The microfolds and microvilli were subsequently severed by the same process of strangulation at the base (Fig. 9a–d) so that, at E20, the epithelium had thinned to approximately 1 μm and was virtually devoid of microvilli (Fig. 9e,f).

As depicted in Figure 10, cells that were immunoreactive for α-SMA (α-smooth muscle actin) formed a subepithelial layer surrounding the parabronchi (Fig. 10a). The latter layer then became discontinuous, forming gaps that delineated the migration routes for the formative atria. The first epithelial colonies started to emerge through the gaps between the α-SMA–positive cells by E12 (Fig. 10b). The number of epithelial cells in the invading colonies increased deep into the surrounding mesenchyme (Fig. 10c,d). The invasion process was accomplished by E16, and the epithelial cells reduced in height forming a lumen and covering the formative atria as a monolayer (Fig. 10e,f). At 2 to 3 days before hatching, the large atria were separated by thin septa and were wide open. The tips of the interatrial septa were supported by the α-SMA–positive cells, and their epithelia spread out into the mesenchyme, giving rise to the infundibula (Fig. 10g,h). Immediately before hatching, the number of α-SMA–positive cells was reduced so that they were restricted to the tips of the interatrial septa.

The number of apoptotic epithelial cells during the whole period of chick lung development remained remarkably negligible. Incidentally, apoptotic epithelial cells were not encountered, which means that programmed cell death was not one of the mechanisms of epithelial attenuation. Isolated apoptotic cells were observed during the entire embryonic period in the mesenchyme with the number of such cells increasing between E14 to E18, a period associated with mesen-

chymal reduction during atria and air capillary formation (Fig. 11). These were located in the mesenchyme ahead of the migrating epithelial tubes, including parabronchi, atria, and also in the walls of developing blood vessels.

DISCUSSION

The avian lung has a volume, which is only three quarters that of mammals of comparable size, whereas the gas exchange surface area is 15% greater (Maina et al., 1989). For corporate data of different avian families, see Duncker and Guentert (1985) and Duncker (2000). This means that, during lung development, the bird has to pack more surface area in a smaller noncompliant lung. This phenomenon calls for ingenious mechanisms of cell attenuation. Notably, the air capillaries in birds grow by radiating into the mesenchymal tissue (Maina, 2004), quite unlike the alveoli in mammalian lungs, which are formed by successive and alternating phases of air space expansion and septation (Pohland, 1986; Duncker, 1990; Makanya et al., 2001; Schittny and Burri, 2003).

Epithelial Attenuation During Mammalian Lung Development

In mammalian lungs, the thin blood–gas barrier is formed by conversion of type II cells to type I cells (Kauffman et al., 1974; Mercurio and Rhodin, 1976, 1978; Makanya et al., 2001). Putative superfluous cells are lost through apoptosis (Schittny et al., 1998; Stiles et al., 2001). Additionally, interstitial tissue diminution brings the capillary endothelium closer to the alveolar epithelium and, in this way, accomplishes a thin blood–gas barrier, which is requisite for efficient gas exchange (Burri and Weibel, 1977; Makanya et al., 2001; Burri et al., 2003). In the developing rat lung, attenuation during pseudoglandular stage inaugurates with shifting of tight junctions from apical regions toward the cell base (Burri and Weibel, 1977; Burri and Moschopulos, 1992). However, mechanisms governing formation of the thin barrier are poorly understood (Duncker, 2000; Schittny

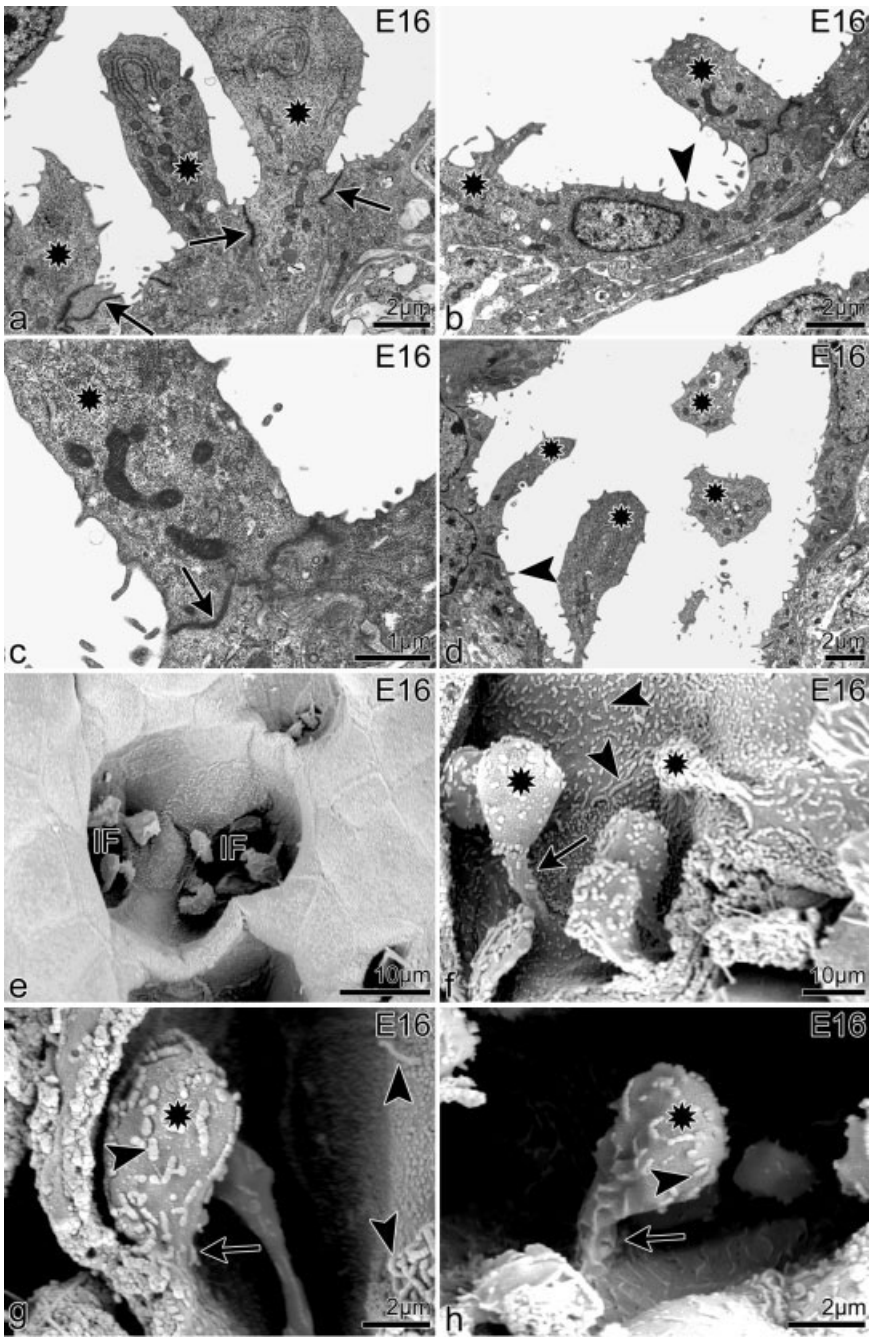

Fig. 6. Transmission (a–d) and scanning (e–h) electron photomicrographs illustrating the various mechanisms involved in attenuation of the gas exchange epithelia during development of the infundibula and air capillaries at E16. **a–d:** The epithelium lining the forming atria and infundibula was of a low cuboidal type. Some of the cells sent long apical processes into the lumen (asterisks). Electron-dense bands (double membranes) then developed at the bases of the projections (arrows in a, c). The two leaves of the double membrane subsequently separated in the formation of cell attenuation bodies. Short microvilli (arrowheads in b, d) were conspicuous at this stage. **e–h:** Scanning electron photomicrographs showing a zoom-in on the club-like intraluminal cell processes encountered during formation of the infundibula (If). These processes were mainly at the base of the atria, whereas the rest of the epithelium was generally flattened. The processes had a rounded apical part (asterisks in f, g, h), and a remarkably narrowed basal part (arrows). Numerous microvilli and microfolds (arrowheads) were typical on the apical projections and the rest of the cell surface.

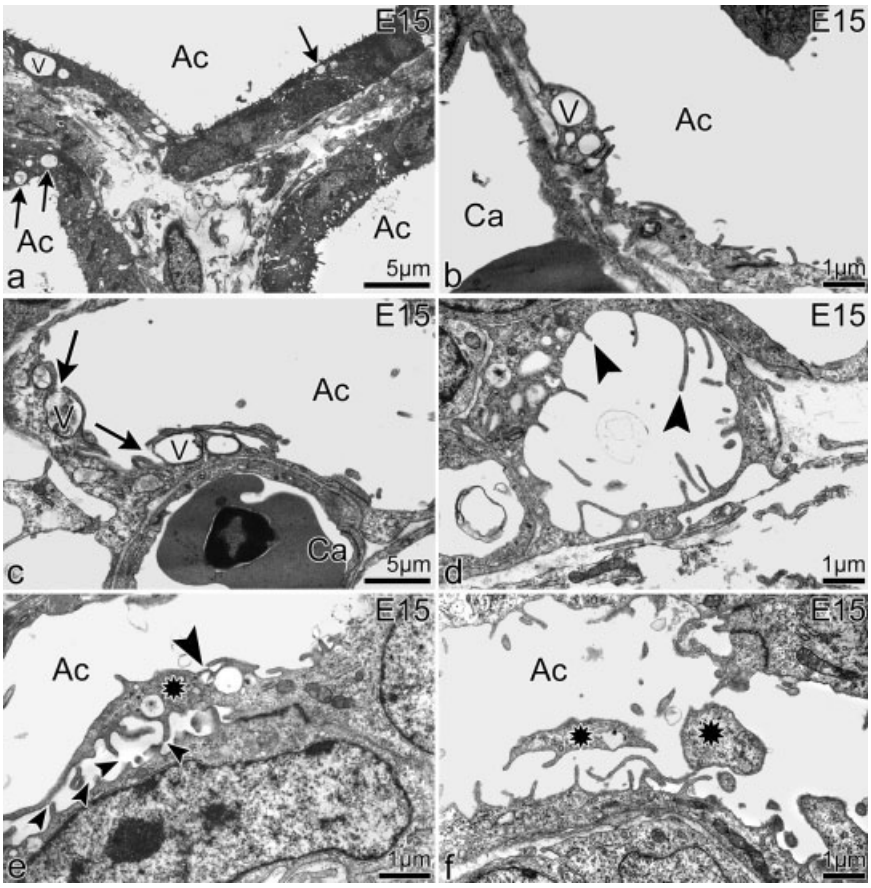

Fig. 7. Transmission electron photomicrographs illustrating the additional mechanisms of epithelial attenuation that occur as from E15. **a–d:** From embryonic day 15 (E15), the process of cell attenuation entailed formation of many large and small vacuoles or vesicles (V and small arrows in a respectively) in the epithelium. In subsequent steps, the vacuoles enlarged (V in b) and fused with the apicolateral plasma membrane (V and arrows in C) and in so doing, left microfolds and microvilli of varying shapes and sizes (arrowheads in d). Ac denotes air capillaries, whereas Ca stands for blood capillaries. Note the varied heights and distribution of the apical cell projections (see arrowheads in d), quite unlike microvilli found in epithelia. **e,f:** In an alternative step, contiguous vacuoles coalesced and fused with their neighboring cognates (arrowheads in e) and, in so doing, cut off large parts of the apical portions of the cells (asterisks in e, f). Although the events described above cannot be unequivocally demonstrated on still pictures, the appearance of vacuoles and vesicles (a–c), their subsequent disappearance and formation of microvilli and microfolds (d) and formation of intraluminal blebs (f), plausibly depict the processes of secarecytosis by vacuolation and vesiculation.

and Burri, 2003). It has been shown that extrusion of lamellar bodies and stretching of the type II cells (Makanya et al., 2001) contribute to formation of the squamous pneumocytes. Notably, programmed cell death was not one of the mechanisms employed by the avian lung during development. Mechanical forces are important for fetal alveolar epithelial cell differentiation. However, the signal transduction pathways regulating this process and the genetic mechanisms and molecules governing epithelial differentiation remain largely unknown.

Epithelial Attenuation During Avian Lung Development

The chick lung undergoes dramatic embryonic development resulting in a complex system of conducting airways and gas exchanging compartments (Figs. 1, 2). The mechanisms underlying the formation of the remarkably thin blood–gas barrier seen in the adult avian lung has, for a long time, remained enigmatic. The findings in the current study indicate that the avian lung uses mechanisms closely related to those of exocrine secretion, albeit in a programmed, time-limited manner. In general, they result in cutting or decapitation of the cell until the required thickness is attained. In the first step, the high columnar epithelium undergoes dramatic size reduction and loses morphological polarization by two main processes: secarecytosis (cell decapitation by cutting) and peremerecytosis (cell decapitation by squeezing, spontaneous constriction, or pinching off). Alternating and successive steps of secarecytosis and peremerecytosis reduce the epithelial height.

Secarecytosis: Cell Attenuation by Cutting

Here, we collectively describe the processes that entail cell cutting under one proposed name, *secarecytosis*, adopted from the Latin word, *secare*, which means to cut. Secarecytosis is a process of cell cutting and subsequent liberation of the apical cellular part, which leads to the reduction in cell height. It has at least two facets: cell double-membrane formation followed by separation between such membranes or cell cutting by vesiculation and/or vacuolation.

Secarecytosis by double membrane formation.

This process starts by E8 so that an apical portion of the polarized cells protrudes into the lumen (Fig. 3). Simultaneously, there is shifting of lateral cell junctions basally so that the apical intercellular spaces open, clearly delineating the apical projection. Subsequently, a transcellular double membrane forms to separate the apical from the basal part. A gap develops between the membranes progressively separating the apical and basal portions of the cell with the result that the apical part of the cell is released into the lumen (see Fig. 3 and also Figs. 11–14 in Testa-Riva and Puxeddu, 1980). This process generally leads to formation of intraluminal blebs of varied shapes and sizes. Early during development (E11–E14), the blebs were notably rounded and closely resembled those of aposecretion, safe for the presence of organelles in the rounded aposomal bodies. Although this process occurs predominantly during the earlier

stages of cell attenuation, it continues at a lower level during the entire embryonic development. Formation of tubules above the dividing membrane parallel to the membrane probably leads to separation of the aposome from the basal part of the cell. A similar phenomenon has been described in apocrine glands, where tubules form parallel to and above the membranes and the subsequent detachment of the protrusion occurs (Schaumburg-Lever and Lever, 1975; Hashimoto, 1978; Zeller and Richter, 1990; Gesase and Satoh, 2003). Positive staining for f-actin at the interphase between the protruding aposome and the basal part of the cell strongly supports this hypothesis for the developing lung epithelium (see Fig. 4).

Secarecytosis by coalescing vesiculation and vacuolation.

The quintessence of decapitation by vesiculation is formation of vesicles in rows below the cell portion to be severed. Such vesicles (endocytic cavities smaller than 50 nm in diameter) finally fuse with their neighboring cognates and then with apicolateral plasma membrane and, in so doing, sever the aposomal projection from the rest of the cell (see Fig. 7). This process occurs much later and appears to target mainly attenuation of the low cuboidal epithelium in the formative atria as well as in the migrating air capillaries. Notably, the released aposomal bodies contained abundant organelles and had several microfolds. Plausibly, the microvilli/microfolds resulted from the fusion of contiguous vesicular membranes (see Figs. 6, 7e,f), at the interphase between the aposome and the basal part of the cell, hence discharging the aposome. Similar demarcating vesicles have been reported during aposecretion in exocrine glands (Smith and Hearn, 1979; Gesase et al., 1996; Gesase and Satoh, 2003), with the notion that the demarcating vesicles were morphologically different from secretory vesicles (Smith and Hearn, 1979). Secarecytosis by coalescing vacuolation is similar to the processes described above, the difference being in the size of the participating endocytic cavities (greater than 50 nm in diameter). This process is contemporaneous with secarecytosis by vesiculation and mainly attenuates the low cuboidal epithelium in the formative atria as well as in the migrating infundibula and air capillaries. Notably, the released aposomal bodies contained abundant organelles and had several microvilli. The microvilli/microfolds resulted from the fusion of contiguous vacuoles, as may be deduced from the thin membranes separating contiguous vacuoles. A similar process has been described by Satoh et al. (1992) and Gesase et al. (1995), which was dubbed "massive exocytosis" due to the absence of apical protrusions that are characteristic of classic aposecretion. This process was later qualified to nonprotrusion aposecretion by Gesase and Satoh (2003), because portions of the cytoplasm trapped between vesicles were released into the glandular lumen, leaving cup-like concavities.

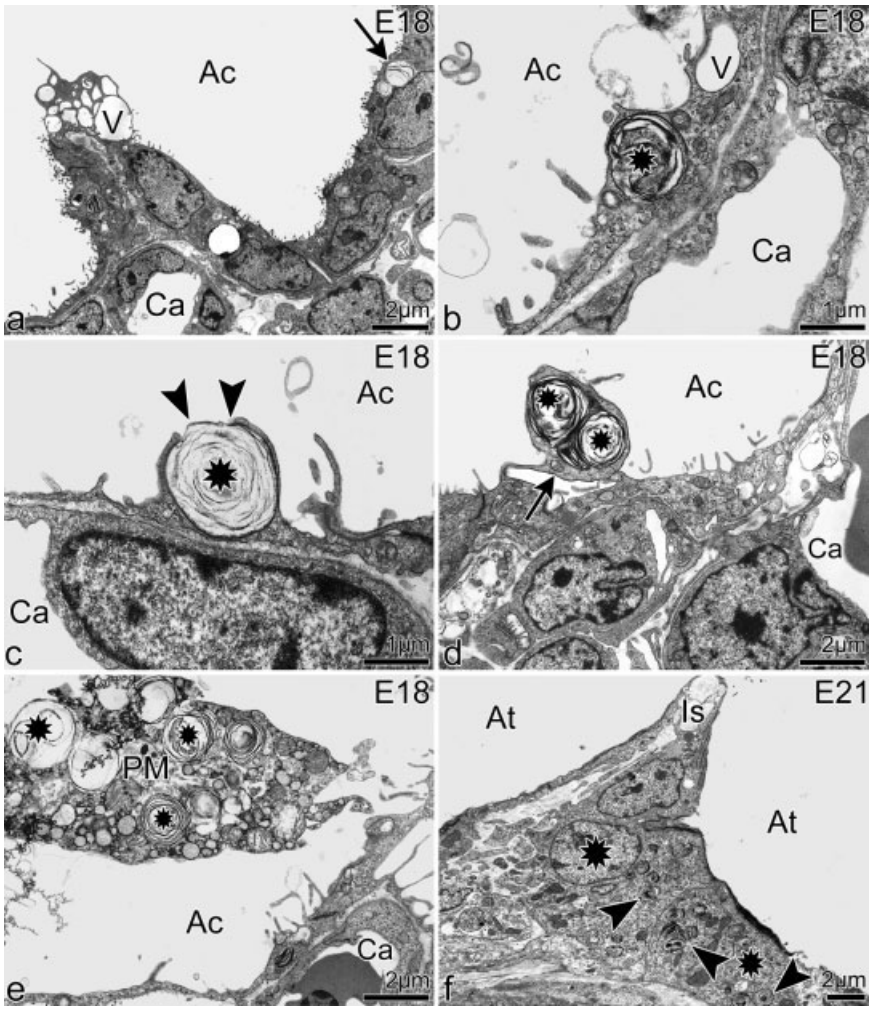

Fig. 8. Transmission electron photomicrographs illustrating the mechanisms involved in cell attenuation during conversion of the granular pneumocytes (type II cells) to squamous pneumocytes. Air capillaries are denoted *Ac* and blood capillaries *Ca*. **a–c:** The epithelia of air capillaries at embryonic day 18 (E18) still contained many lamellar bodies (arrow in a and asterisks in b, c,). Such lamellar bodies were extruded by bulging onto the apical plasma membrane with subsequent rupture of the membrane (arrowheads in c). The process of attenuation by rupturing vacuolation (see V in a and b) entailed development of vacuoles and fusion of their membranes with apical plasma membrane with subsequent release of vacuolar contents. **d:** An alternative method of eliminating lamellar bodies entailed formation of vacuoles beneath the lamellar bodies with subsequent rupture of the vacuoles (arrow), so that the lamellar bodies were discharged together with part of the cytoplasm. **e:** The cellular debris and the resultant lamellar bodies (asterisks) discharged into the lumen were plausibly cleared by pulmonary macrophages (PM), as may be inferred from the presence of numerous lamellar bodies in the latter cell. **f:** In the later stages of development of the maturing lung, the type II cells (asterisks) with lamellar bodies (arrowheads) were confined to the atrial region only. *At*, atria separated by interatrial septa.

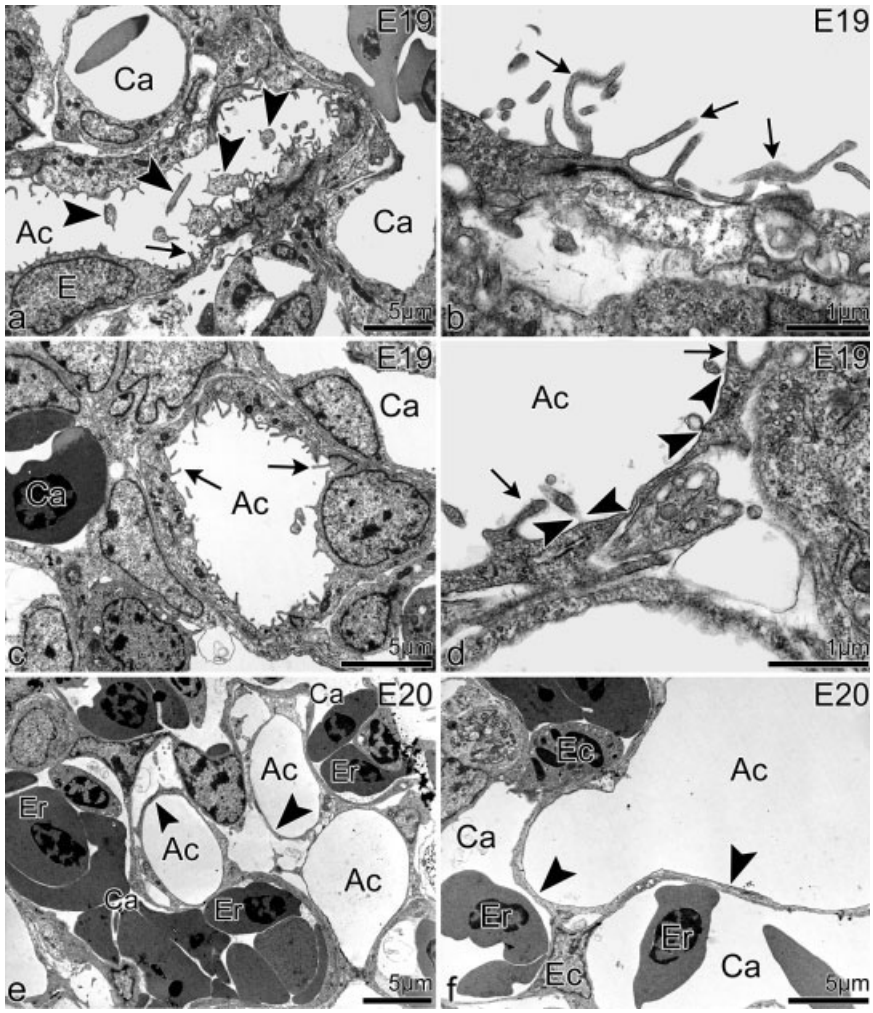

Fig. 9. Transmission electron photomicrographs showing the terminal mechanisms involved in cell attenuation during the development of a thin blood–gas barrier. **a,b:** Continued vesiculation and vacuolation, fusion, and rupture of vacuoles and vesicles resulted in numerous cell attenuation bodies of varied sizes and shapes (arrowheads in a) within the air capillaries (Ac) as well as microfolds and microvilli of irregular shapes and sizes (arrows). The blood capillaries (Ca) approached the thinning epithelium (E) to form a thin blood–gas barrier. **c,d:** The cell attenuation bodies became fewer in air capillaries (Ac) by embryonic day 19 (E19), and the microfolds and microvilli (arrows) were reduced in number and much shorter. Notice the blood capillaries (Ca) now approximated the air capillaries (Ac) epithelium to form the thin blood–gas barrier. The microfolds and microvilli were severed by the process of spontaneous strangulation (arrowheads in d). **e,f:** By E20, there were virtually no microfolds or microvilli. The mesenchyme was reduced, and numerous air capillaries (Ac) were closely apposed to blood capillaries (Ca) forming a thin blood–gas barrier (arrowheads e). All the microvilli and microfolds had disappeared so that the only distinguishing feature between the air capillaries and the blood capillaries was the presence of red blood cells (Er) in the latter. EC, endothelial cell.

Secarecytosis by Rupturing Vacuolation and Vesiculation

In this case, vacuoles (membrane bound cavities larger than 50 nm in diameter) are formed at the apical part of the cell, the vacuoles enlarge, putatively by accumulation of fluid from the cell and, therefore, tend to protrude toward the lumen above the general cell surface, then the vacuolar membrane fuses with the apical plasma membrane, releasing its contents into the lumen and forming shallow concavities separated by microfolds and microvilli. Alternatively, the cell may form vesicles (tiny vacuoles less than 50 nm in diameter) in a designated region. Fusion of such vesicles with the apical plasma membrane results in rupture and formation of tiny microvilli but with concomitant reduction in cell height. The microfolds/microvilli formed as a result of vacuolation and vesiculations are then severed by progressive thinning and constriction at the base with ultimate formation of a smooth, squamous epithelium (Fig. 9). Successive phases of formation of such vacuoles and vesicles, their rupture, consequent formation, and severance of microvilli plausibly discharges substantial portions of the fluid and solid portions of the cell so that, at the time of hatching, the respiratory epithelium is thin, smooth, and squamous.

Physiological secretion during exocytosis is known to occur through fusion of the vesicular membrane with the apical cell membrane forming small pores (Kliewer et al., 1985). However, during secarecytosis by rupturing vacuolation, the fusion of the vacuole membrane with the apical plasma membrane results in rupture of the vacuole, discharge of the entire contents, and formation of microvilli and microfolds, as may be deduced from the disappearance of the vacuoles and the resultant microvilli and microfolds. Notably, numerous microvilli are formed during secarecytosis, but such are noted to disappear during both apocrine and nonapocrine secretion (Gesase and Satoh, 2003). Decapitation of microvilli during avian lung development occurs as a final step, through constriction at the base.

Peremerecytosis: Cell Decapitation by Squeezing, Constriction, or Pinching Off

Peremerecytosis is morphologically distinguished by apical club-like cell protrusions (see Figs. 3, 6). In spontaneous peremerecytosis, the cells become tapered, intercellular spaces between the apical parts of the cells widen, and the cells become constricted at the supranuclear region until the apical part is squeezed out. In some cases the better-endowed cognate neighbors squeeze a sandwiched cell out until the apical portion is ejected. In either case, progressive thinning of the stalk of the protrusion results in severing of the aposome. Aposecretion by pinching off has been described in glands (Gesase and Satoh, 2003). Classic aposecretion is characterized by bulging of the apical cytoplasm, absence of subcellular structures, and presence of membrane bound cell fragments, the so-called aposomes (Deyrup-Olsen and Luchtel, 1998). However,

this differs from the current observations in that the decapitated portion of the cells during development contains major organelles; sometimes an entire cell is squeezed out. The mechanisms that cause thinning of the aposomal stalk are unknown (Gesase and Satoh, 2003), but actin filaments are probably involved (Metzler et al., 1992; Aumuller et al., 1999; Stoeckelhuber et al., 2000, see also Fig. 4).

Role of α-SMA–Positive Cells During Parabronchial Development

The establishment of a thin blood–gas barrier occurs concomitantly with parabronchial expansion and formation of atria, infundibula, and air capillaries. Early during development (E8) α-SMA–positive cells become associated with the basal aspects of parabronchial epithelial cells and surround the latter. However, such cells are interrupted by gaps through which the formative atria sprout. As soon as the atria are patterned, the α-SMA staining intensity declines dramatically, probably due to the reduction of α-SMA–positive cells by apoptosis and/or their transformation to fibroblasts. The driving mechanisms involved in the pattering of α-SMA–positive cells are at the moment unclear. Putatively, α-SMA–positive cells participate in the patterning of the formative atria but finally are restricted to supporting the interatrial septa in the prehatch embryo.

Contractile cells have been associated with apocrine and holocrine secretion (Aumuller et al., 1999). During milk secretion, for example, myoepithelial cells are known to squeeze the secretory epithelium and, in so doing, facilitate the release of milk into the secretory acinus (Furuya et al., 2004; Macuhova et al., 2004). The association of α-SMA–positive cells with the parabronchial epithelium during the time of secarecytosis and peremerecytosis probably is important in facilitating these aposecretion-like cell attenuation processes.

Putative Mechanisms in Physiological Secretion, Secarecytosis, and Peremerecytosis

Mechanisms in aposecretion have been reviewed recently by Gesase and

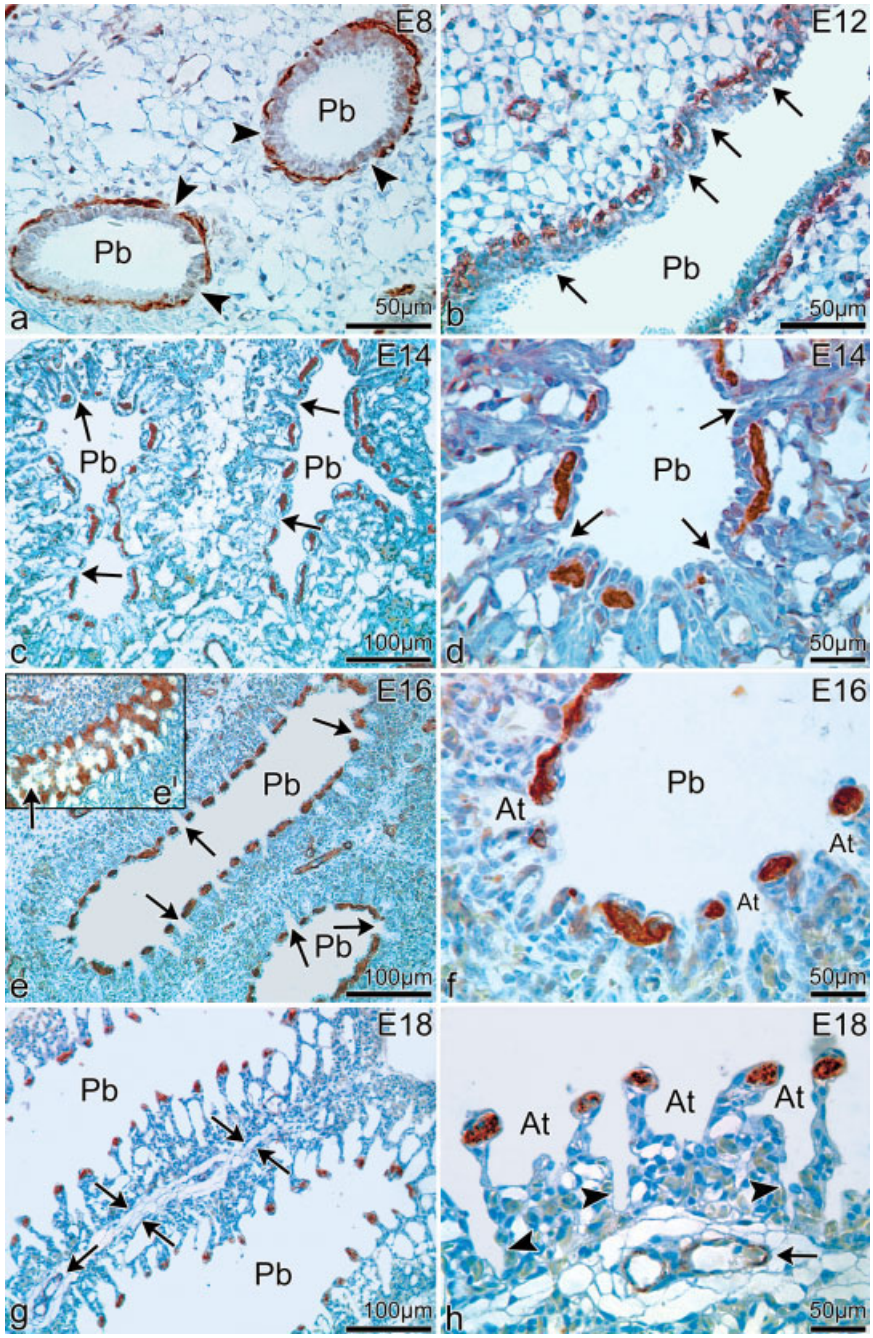

Fig. 10. Immunohistochemical staining (dark brown coloration) for α-SMA (α-smooth muscle actin, a protein found in smooth muscle cells) of lung specimens at different developmental stages. **a,b:** At the formative stages of the parabronchi (embryonic day 8, E8), the epithelium was surrounded by a layer of α-SMA–positive mesenchymal cells interrupted by intervening gaps (arrowheads in a). By E12 (b), the gaps between the α-SMA–positive cells were smaller but occurred more frequently and were more regularly spaced. The first strands of migrating epithelial cells (arrows in b), which represented the sprouting atria, invaded the mesenchyme through gaps delineated by the α-SMA–positive cells. **c,d:** By E14, columns of parabronchial epithelial cells had penetrated deeper into the surrounding mesenchyme (arrows). Note that d is an inset of c at higher magnification showing the migrating atrial cells (arrows). **e,f:** The atria (At) at E16 formed through the gaps between the α-SMA–positive cells (arrows in e), and the latter cells marked the incipient interatrial septa.. The α-SMA–positive cells formed a network or honeycomb-like pattern surrounding the parabronchus as depicted in e′ (inset). At a higher magnification (f), the formative atria (At) opening into the parabronchial lumen (Pb) were clearly delineated by the dark staining immunopositive cells. **g,h:** By E18 (g,h), the interparabronchial septum was thin (arrows in g) but well endowed with blood capillaries. The atria (At in h) were well formed, continuous with the infundibula (arrowheads in h), and separated by prominent interatrial septa whose tips were reinforced with α-SMA–positive cells (arrows in h). Pb denotes parabronchial lumina. Note that h is an inset of e at a higher magnification.

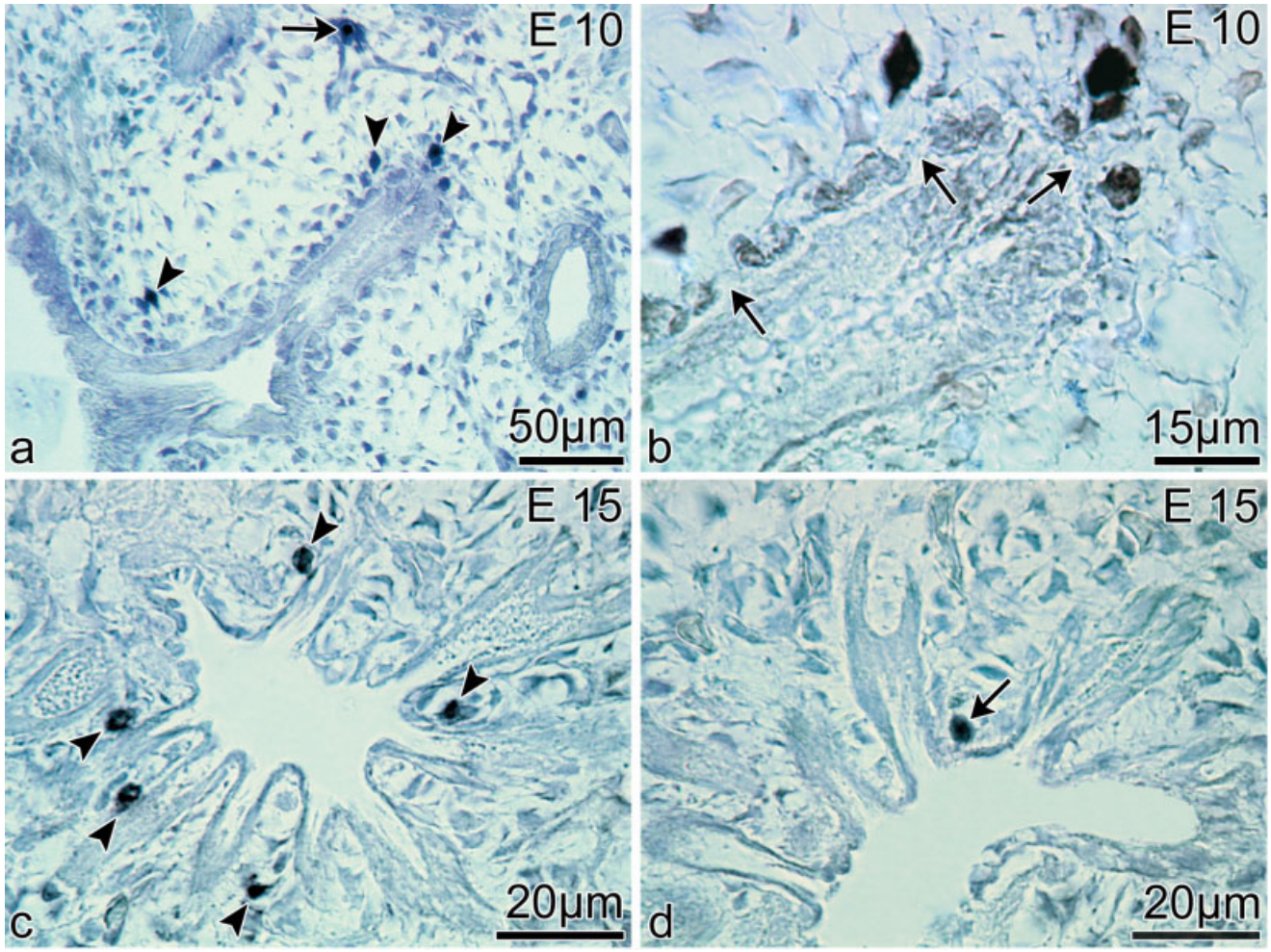

Fig. 11. Terminal transferase-mediated dUTP nick-end labeling (TUNEL) assay illustrating the type and location of the dying cells (dark coloration) during chick embryo lung development. **a,b:** At embryonic day 10 (E10), the apoptotic cells were localized in the mesenchyme surrounding the parabronchi (arrowheads) or occasionally in the blood vessels (arrow). At higher magnification, it was obvious that they occurred in the regions between the α-smooth muscle actin–positive cells, which were the passageways for the sprouting atrial tubes (arrows). **c,d:** At E15, the apoptotic cells were located in the mesenchymal tissue between the atria (arrowheads) and seldom at the tip of the interatrial septa (arrow).

Satoh (2003), with the notion that the biochemical and physiological pathways regulating aposecretion as well as the plasma membrane dynamics are poorly understood. This is complicated by the fact that, in most occasions, aposecretion is accompanied by exocytosis. Physiological release of surfactant occurs through elliptical cell surface pores averaging 0.2 × 0.4 microns in size on the alveolar luminal side of type II cells. In the attenuating epithelium of the chicken lung, entire lamellar bodies were released either through large apical pores or together with part of the cytoplasm by abscising vacuolation (secarecytosis).

The plasma membrane dynamics during apocrine secretion have not been extensively investigated (Gesase and Satoh, 2003). Participation of cytoskeletal proteins, such as myosin and gelsolin (Aumuller et al., 1999) or even actin (Stoeckelhuber et al., 2003) in the pinching off of the apical protrusion during aposecretion has been implicated. In the chick embryo lung, the presence of actin filaments in the constricting aposome has been demonstrated in the current study. These actin filaments putatively participate in aposomal constriction during peremerecytosis. Furthermore, actin filaments are known to be associated with the cell adhesion belt (Volberg et al., 1986) and, in the current study, have been used as indicators for distal relocation of cell junctions. During embryonic development, ingressing cells are known to change shape and their apices constrict, putatively through actinomyosin contraction (Shook and Keller, 2003). Such a constriction displaces the organelles basally in readiness for migration (Shook and Keller, 2003). Physiologically, aposecretion is archetypical in the reproductive system and is controlled by hormones and muscarinic innervation (Aumuller et al., 1999). Apparently, formation of the thin blood–gas barrier in the avian lung follows mechanisms different from those reported for mammals.

Apoptosis and Formation of the Thin Blood–Gas Barrier

It is obvious, that active cell death is not directly involved in the attenuation of the chicken lung epithelium. Despite this finding, the process is very important in the formation of the thin blood–gas barrier. The dying

mesenchymal cells give way to the expanding and migrating epithelial tubes. Putatively, this process has a precise temporospatial regulation. It is intriguing how the mesenchymal cells immediately ahead of the migrating epithelial tubes become the initial targets of apoptosis. During atria formation, mesenchymal cell apoptosis is responsible for diminution of the interstitium between the epithelial tubes and, hence, participates in the approximation and subsequent apposition of the attenuated epithelium to the capillary endothelium and the ultimate establishment of a very thin blood–gas barrier.

EXPERIMENTAL PROCEDURES

Experimental Animals

Brown Leghorn eggs were incubated at 37°C and a humidity of 65%. Embryos covering Hamburger and Hamilton stages 19 to 45 were obtained and processed according to the methods described below.

Microscopy

For both light microscopy and transmission electron microscopic studies, lungs were fixed using a solution of 2.5% glutaraldehyde in 0.1 M cacodylate buffer (pH 7.4, 350 mOsm). Tissue blocks were postfixed in osmium tetroxide, block-stained using uranyl acetate, dehydrated through ascending concentrations of ethanol, and embedded in epoxy resin. Semithin sections were obtained at a nominal thickness of 5 μm, stained with toluidine blue, and viewed under a Leica or Coolscope light microscope. Ultrathin sections were obtained at 90 nm, counterstained with lead citrate, and viewed on a Philips EM-300 microscope. For the scanning electron microscopy, the lungs were fixed by intratracheal infusion of the same fixative as above or total immersion of the specimen into the fixative. Selected lung specimens were dehydrated through ascending concentrations of ethanol, critical point-dried in liquid carbon dioxide, and mounted on aluminium stubs. The specimens were sputter-coated with gold and viewed under a Philips XL 30 FEG scanning electron microscope.

Immunohistochemistry for α-SMA

Specimens destined for immunohistochemistry were fixed by intratracheal infusion of 4% paraformaldehyde, or total immersion into the same fixative, rinsed in 15% sucrose solution, and then stored in 70% ethanol. Tissue blocks were embedded in parafin wax and sections were obtained at a nominal thickness of 3 μm. Paraffin sections were transferred to gelatinized microslides and air-dried overnight at 37°C. They were dewaxed in xylene (three changes), rehydrated in graded series of ethanol, and rinsed twice in Tris-buffered saline (TBS) 50 mM Tris/HCl (pH 7.4), containing 100 mM sodium chloride. After incubation with the first antibody diluted in TBS, mouse anti-SMA (1:200; Sigma, Buchs, Switzerland), sections were exposed to an affinity-purified biotinylated second antibody (anti-mouse EO 433, Dako; Glostrup, Denmark; diluted 1:200 in TBS) for 45 min at ambient temperature, washed three times in TBS, then treated with the avidin–biotin–horseradish peroxidase complex (P355, Dako, Glostrup, Denmark) for a similar period. The reaction products were visualized by exposing the sections to 3-amino-9-ethylcarbazole or 3,3-diaminobenzidine (Sigma Chemicals Company, St. Louis, MO) for 10 min. Negative controls were prepared using nonspecific mouse sera.

Terminal Transferase-Mediated dUTP Nick-End Labeling Assay

The terminal transferase-mediated dUTP nick-end labeling (TUNEL) assay is used as a marker of apoptosis. The method applied is based upon that described by Schittny et al. (1998). Briefly, 3-μm-thick paraffin-embedded sections were dewaxed in xylene (three changes), rehydrated in ethanol, rinsed twice in TBS, and incubated in a solution of proteinase K (20 μg/ml of TBS) for 15 min at ambient temperature. Endogenous peroxidase activity was suppressed by treatment with 0.3% hydrogen peroxide for 10 min at ambient temperature. The sections were then incubated first with terminal deoxynucleotidyl transferase (TdT) for 60 min at 37°C and then with a peroxidase-conjugated anti-digoxigenin antibody for 30 min at ambient temperature. The reaction was visualized by exposing sections to the enzyme substrate diaminobenzidine for 8 min at ambient temperature.

Alexa–Phalloidin Staining for F-actin

Chick embryo lungs were dissected out on E12, snap frozen in isopentane, and cooled in liquid nitrogen. Cryostat sections (8 μm) were prepared and incubated for 30 min with Alexa fluor–phalloidin 488 (Molecular Probes) diluted 1:500 in phosphate-buffered saline (PBS). After a rinse in PBS, the sections were fixed in 4% paraformaldehyde in HEPES buffer and then washed and mounted in gelvatol. The specimens were viewed in a ZEISS LSM Meta 510 confocal microscope.

ACKNOWLEDGMENTS

We thank Krystyna Sala, Bettina de Breuyn, and Barbara Krieger for their technical support.

REFERENCES

Aumuller G, Wilhelm B, Seitz J. 1999. Apocrine secretion—fact or artifact? Anat Anz 181:437–446.

Bellairs R, Osmond M. 1998. The atlas of chick development. London: Academic Press.

Burri PH, Moschopulos M. 1992. Structural analysis of fetal rat lung development. Anat Rec 234:399–418.

Burri PH, Weibel ER. 1977. Ultrastructure and morphometry of the developing lung. In: Hodson WA, editor. Development of the lung. New York and Basel: M. Dekker, Inc. p 215–268.

Burri PH, Haenni B, Tschanz SA, Makanya AN. 2003. Morphometry and allometry of the postnatal marsupial lung development: an ultrastructural study. Respir Physiol Neurobiol 138:309–324.

Deyrup-Olsen I, Luchtel DL. 1998. Secretion of mucous granules and other membrane-bound structures: a look beyond exocytosis. Int Rev Cytol 183:95–141.

Duncker HR. 1971. The lung air sac system of birds. A contribution to the functional anatomy of the respiratory apparatus. Ergeb Anat Entwicklungsgesch 45:7–171.

Duncker HR. 1978. [Coelom organization of vertebrates—functional aspects]. Verh Anat Ges 91–112.

Duncker HR. 1990. 21. Respirationstrakt. In: Hinrichsen KV, editor. Human-Embryologie. Berlin: Springer. p 571–606.

Duncker HR. 2000. Der Atemapparat der Vögel und ihre lokomotorische und metabolische Leistungsfähigkeit. J Ornithol 141:1– 67.

Duncker HR, Guentert M. 1985. The quantitative design of the avian respiratory system from hummingbird to mute swan. In: Nachtigall W, editor. Bionareport 3: Bird flight Vogelflug. Stuttgart: Fischer. p 361–378.

Furuya K, Akita K, Sokabe M. 2004. [Extracellular ATP mediated mechano-signaling in mammary glands]. Nippon Yakurigaku Zasshi 123:397–402.

Gallagher BC. 1986a. Basal laminar thinning in branching morphogenesis of the chick lung as demonstrated by lectin probes. J Embryol Exp Morphol 94:173–188.

Gallagher BC. 1986b. Branching morphogenesis in the avian lung: electron microscopic studies using cationic dyes. J Embryol Exp Morphol 94:189–205.

Gesase AP, Satoh Y. 2003. Apocrine secretory mechanism: recent findings and unresolved problems. Histol Histopathol 18: 597–608.

Gesase AP, Satoh Y, Ono K. 1995. G-protein activation enhances Ca(2+)-dependent lipid secretion of the rat harderian gland. Anat Embryol (Berl) 192:319–328.

Gesase AP, Satoh Y, Ono K. 1996. Secretagogue-induced apocrine secretion in the Harderian gland of the rat. Cell Tissue Res 285:501–507.

Hashimoto K. 1978. The apocrine gland. In: Jarret A, editor. The physiology and pathophysiology of the skin. Vol. 5. London: Academic Press. p 1575–1596.

Jones AW, Radnor CJ. 1972. The development of the chick tertiary bronchus. I. General development and the mode of production of the osmiophilic inclusion body. J Anat 113:303–324.

Kalenga M, Tschanz SA, Burri PH. 1995. Protein deficiency and the growing rat lung. II. Morphometric analysis and morphology. Pediatr Res 37:789–795.

Kauffman SL, Burri PH, Weibel ER. 1974. The postnatal growth of the rat lung. II. Autoradiography. Anat Rec 180:63–76.

King AS, McLelland J, editors. 1989. Form and function in birds. Vol. 4. London: Academic Press.

Kliewer M, Fram EK, Brody AR, Young SL. 1985. Secretion of surfactant by rat alveolar type II cells: morphometric analysis and three-dimensional reconstruction. Exp Lung Res 9:351–361.

Macuhova J, Tancin V, Bruckmaier RM. 2004. Effects of oxytocin administration on oxytocin release and milk ejection. J Dairy Sci 87:1236–1244.

Maina JN. 2003a. A systematic study of the development of the airway (bronchial) system of the avian lung from days 3 to 26 of embryogenesis: a transmission electron microscopic study on the domestic fowl, *Gallus gallus variant domesticus*. Tissue Cell 35:375–391.

Maina JN. 2003b. Developmental dynamics of the bronchial (airway) and air sac systems of the avian respiratory system from day 3 to day 26 of life: a scanning electron microscopic study of the domestic fowl, *Gallus gallus variant domesticus*. Anat Embryol (Berl) 207:119–134.

Maina JN. 2004. Morphogenesis of the laminated, tripartite cytoarchitectural design of the blood-gas barrier of the avian lung: a systematic electron microscopic study on the domestic fowl, *Gallus gallus variant domesticus*. Tissue Cell 36: 129–139.

Maina JN, King AS, Settle G. 1989. An allometric study of pulmonary morphometric parameters in birds, with mammalian comparisons. Philos Trans R Soc Lond B Biol Sci 326:1–57.

Makanya AN, Sparrow MP, Warui CN, Mwangi DK, Burri PH. 2001. Morphological analysis of the postnatally developing marsupial lung: the quokka wallaby. Anat Rec 262:253–265.

Mercurio AR, Rhodin JAG. 1976. An electron microscopic study on the type I pneumocyte in the cat: differentiation. Am J Anat 146:255–272.

Mercurio AR, Rhodin JAG. 1978. An electron microscopic study on the type I pneumocyte in the cat: pre-natal morphogenesis. J Morphol 156:141–156.

Metzler G, Schaumburg-Lever G, Fehrenbacher B, Moller H. 1992. Ultrastructural localization of actin in normal human skin. Arch Dermatol Res 284:242–245.

Pohland DW. 1986. Die Entwicklung des respiratorischen Bronchialbaums und die Entstehung der Alveolen bei Meerschweinchen und Schaf. Med Diss Giessen.

Satoh Y, Ishikawa K, Oomori Y, Takede S, Ono K. 1992. Secretion mode of the harderian gland of rats after stimulation by cholinergic secretagogues. Acta Anat (Basel) 143:7–13.

Schaumburg-Lever G, Lever WF. 1975. Secretion from human apocrine glands: an electron microscopic study. J Invest Dermatol 64:38–41.

Scheuermann DW, Klika E, Groodt-Lasseel MH, Bazantova I, Switka A. 1998. The development and differentiation of the parabronchial unit in quail (*Coturnix coturnix*). Eur J Morphol 36:201–215.

Schittny JC, Burri PH. 2003. Morphogenesis of the mammalian lung: aspects of structure and extracellular matrix components. In: Massaro DJ, Massaro G, Chambon P, editors. Lung development and regeneration. New York: Dekker. p 275–317.

Schittny JC, Djonov V, Fine A, Burri PH. 1998. Programmed cell death contributes to postnatal lung development. Am J Respir Cell Mol Biol 18:786–793.

Shook D, Keller R. 2003. Mechanisms, mechanics and function of epithelial-mesenchymal transitions in early development. Mech Dev 120:1351–1383.

Smith JD, Hearn GW. 1979. Ultrastructure of the apocrine-sebaceous anal scent gland of the woodchuck, *Marmota monax*: evidence for apocrine and mesocrine secretion by a single cell type. Anat Rec 193:269–291.

Stiles AD, Chrysis D, Jarvis HW, Brighton B, Moats-Staats BM. 2001. Programmed cell death in normal fetal rat lung development. Exp Lung Res 27:569–587.

Stoeckelhuber M, Sliwa A, Welsch U. 2000. Histo-physiology of the scent-marking glands of the penile pad, anal pouch, and the forefoot in the aardwolf (*Proteles cristatus*). Anat Rec 259:312–326.

Stoeckelhuber M, Stoeckelhuber BM, Welsch U. 2003. Human glands of Moll: histochemical and ultrastructural characterization of the glands of Moll in the human eyelid. J Invest Dermatol 121:28–36.

Testa-Riva F and Puxeddu P. 1980. Secretory mechanisms of human ceruminous glands: a transmission and scanning electron microscopic study. Anat Rec 196: 363–372.

Volberg T, Geiger B, Kartenbeck J, Franke WW. 1986. Changes in membrane-microfilament interaction in intercellular adherens junctions upon removal of extracellular Ca2+ ions. J Cell Biol 102:1832–1842.

Zeller U, Richter J. 1990. The monoptychic glands of the jugulo-sternal scent gland field of Tupaia: a TEM and SEM study. J Anat 172:25–38.